

An evaluation on mechanisms of miscibility development in acid gas injection for volatile oil reservoirs

Erhui Luo*, Zifei Fan, Yongle Hu, Lun Zhao, and Jianjun Wang

PetroChina Research Institute of Petroleum Exploration & Development, Beijing 100083, China

Received: 25 December 2018 / Accepted: 20 March 2019

Abstract. Produced gas containing the acid gas reinjection is one of the effective enhanced oil recovery methods, not only saving costs of disposing acid gases and zero discharge of greenhouse gases but also supporting reservoir pressure. The subsurface fluid from the Carboniferous carbonate reservoir in the southern margin of the Pre-Caspian basin in Central Asia has low density, low viscosity, high concentrations of H₂S (15%) and CO₂ (4%), high solution gas/oil ratio. The reservoir is lack of fresh water because of being far away onshore. Pilot test has already been implemented for the acid gas reinjection. Firstly, in our work a scheme of crude oil composition grouping with 15 compositions was presented on the basis of bottomhole sampling from DSTs of four wells. After matching PVT physical experiments including viscosity, density and gas/oil ratio and pressure-temperature (*P-T*) phase diagram by tuning critical properties of highly uncertain heavy components, the compositional model with phase behavior was built under meeting accuracy of phase fitting, which was used to evaluate mechanism of miscibility development in the acid gas injection process. Then using a cell-to-cell simulation method, vaporizing and/or condensing gas drive mechanisms were investigated for mixtures consisting of various proportions of CH₄, CO₂ and H₂S in the gas injection process. Moreover, effects of gas compositions on miscible mechanisms have also been determined. With the aid of pressure-composition diagrams and pseudoternary diagrams generated from the Equation of State (EoS), pressures of First Contact Miscibility (FCM) and Multiple Contact Miscibility (MCM) for various gases mixing with the reservoir oil sample under reservoir temperature were calculated. Simulation results show that pressures of FCM are higher than those of MCM, and CO₂ and H₂S are able to reduce the miscible pressure. At the same time, H₂S is stronger. As the CH₄ content increases, both pressures of FCM and MCM are higher. But incremental values of MCM decrease. In addition, calculated envelopes of pseudoternary diagrams for mixtures of CH₄, CO₂ and H₂S gases of varying composition with acid gas injection have features of bell shape, hourglass shape and triangle shape, which can be used to identify vaporizing and/or condensing gas drives. Finally, comparison of the real produced gas and the one deprived of its C₃⁺ was performed to determine types of miscibility and calculate pressures of FCM and MCM. This study provides a theoretical guideline for selection of injection gas to improve miscibility and oil recovery.

1 Introduction

Gas injection is an important enhanced oil recovery process, in which interphase mass transfer during multiple contacting of the injected gas and the reservoir oil results in an efficient displacement. Reinjection into the reservoir of a gas produced from an oil field is commonly used. While the reasons are lack of transport pipelines and saving cost of disposing produced gas, much interest is being devoted to gas injection as an enhanced oil recovery process. Obviously, reinjection of the gas reduces the pressure drop associated with production of oil from a field. Moreover, immiscible/miscible gas injection can occur when the

injected gas diffuses into the oil, and the oil will swell and oil viscosity reduces. If the interfacial tension is eliminated, miscible gas drive occurs. However, the injected gas also affects the oil/gas equilibrium compositions in the reservoir. Injection of various gases involving CO₂ and acid gas into the oil reservoir has been investigated by some authors. There is the miscible HC gas reinjection project with large volumes of sour gas (3–4% H₂S and 10–15% CO₂) at Harweel field in Oman (Al-Hadhrami *et al.*, 2007). The pilot project is a first contact miscible gas injection with 12% H₂S content which has recently been running in the Tengiz oilfield in Kazakhstan (Wang *et al.*, 2014; Urazgaliyeva *et al.*, 2014). CO₂ injection has also made a good progress (Luo *et al.*, 2013a, b).

Miscibility development has two different processes: First Contact Miscibility (FCM) and Multiple Contact

* Corresponding author: luoerhui2006@163.com

Miscibility (MCM). If a single phase is formed when the original oil and the injected gas become fully miscible, the oil and gas phases exhibit FCM. If the original oil and the injected gas need multiple contacts to achieve miscibility, MCM will happen. The traditional interpretation of the MCM indicates that the gas may take up components from the oil phase corresponding to the vaporizing gas drive, the oil may take up components from the gas phase corresponding to the condensing gas drive. Later, a combined vaporizing/condensing mechanism was presented to describe MCM (Zick, 1986; Stalkup, 1987; Johns *et al.*, 2002). Multiple contact experiments were conducted to study the effect of phase behavior on CO₂ flood (Gardner *et al.*, 1981). Abrishami and Hatamian (1996) studied the thermodynamic behavior of hydrocarbon fluids in multiple contact processes with non-hydrocarbon (N₂, CO₂ and their mixtures) through experiments. Ternary diagrams are commonly used to decide whether or not miscibility has been achieved. A cell-to-cell simulation program was presented by Metcalfe *et al.* (1973). Pederson *et al.* (1986) used a cell-to-cell model in connection with a ternary diagram to simulate a miscible drive. Nutakki *et al.* (1991) interpreted the mechanism of oil recovery as a condensing/vaporizing process with significant upper phase extraction on the basis of pseudoternary diagrams and pressure-composition diagrams generated from the Equation of State (EoS). Tang *et al.* (2005) evaluated the miscible ability and mechanism of gas displacement by simulating the PVT experiment data, pressure-composition experiment, multiple contact miscible experiment and slim-tube experiment available. Johns *et al.* (2010) calculated Minimum Miscibility Pressure (MMP) for oils displaced by CO₂ contaminated by mixtures of N₂, CH₄, C₂, C₃, and H₂S. Belhaj *et al.* (2013) evaluated miscible oil recovery utilizing N₂ and/or HC gases in CO₂ injection. It is clear that the major research focuses on CO₂ injection or CO₂ mixtures with other gases, but there are very limited studies on acid gas injection with high H₂S content (Zhang *et al.*, 2017; Luo *et al.*, 2018).

In this paper, a simulation study was conducted to evaluate the performance of the acid gas miscible injection process. Pseudoternary diagrams are used to represent the mixing processes which take place in a petroleum reservoir into which gas is being injected. Mixtures consisting of various proportions of reservoir oil and injection gas (static mixtures of 0 mol%–90 mol% injection gas) were calculated to generate the pressure-composition diagram for the multi-component system. Multiple-contact calculations were then performed at a pressure equal to the flooding pressure and the pseudoternary diagram was generated. The principal mechanisms of the oil recovery were then identified using the many-component pressure-composition diagram and pseudoternary diagram.

2 Phase behavior modeling and PVT matching

2.1 Phase behavior modeling

In order to access the acid gas flooding, the oil samples utilized are from the Carboniferous carbonate reservoir located

in the southern part of the Pri-Caspian basin marginal zone. There are four wells (well X-1, well X-2, well X-3 and well X-6) that have been performed six DSTs to obtain representative bottomhole fluids samples. To make sure the good quality of the sampled fluids, the flowing bottomhole pressure during sampling is larger than the saturation pressure. The routine PVT data includes Constant Mass Expansion (CCE) and Differential Liberation (DL) for the reservoir fluids. The saturation point of the reservoir fluid is found to be 28.4 MPa at 98 °C. Column 2 of Table 1 shows the composition of the reservoir oil sample. The acid gas component (H₂S + CO₂) mole fraction in the oil sample is 19.23%.

The solution Gas-Oil Ratio (GOR) is high (640–670 m³/m³). The produced fluid was separated by the three-stage separator (Fig. 1). The conditions of high pressure, middle pressure and low pressure separators are 9.6 MPa, 3.0 MPa, 8.5 MPa and 70 °C, 60 °C, 52 °C respectively. The produced gas is exported directly to shore except reinjection gas and fuel gas. Because every separator has different pressure and temperature, GOR and H₂S concentration of every separator is varied that leads to the compressor with various gas compositions. Column 3 of Table 1 shows the composition of the produced gas injected into the reservoir. To compare the effect of the gas composition, the produced gas is deprived C₃⁺, named deprived C₃⁺.

2.2 Laboratory PVT data matching

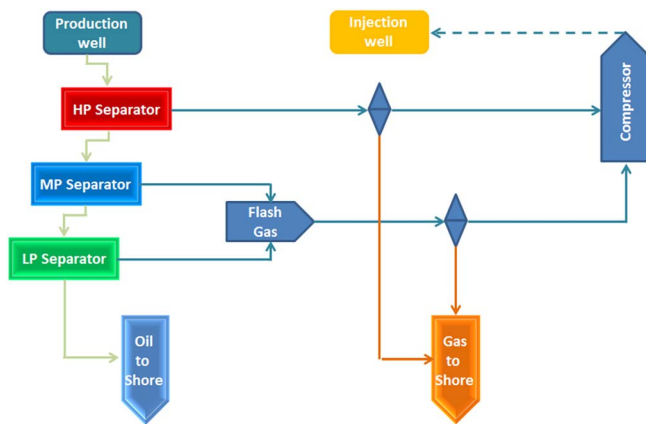
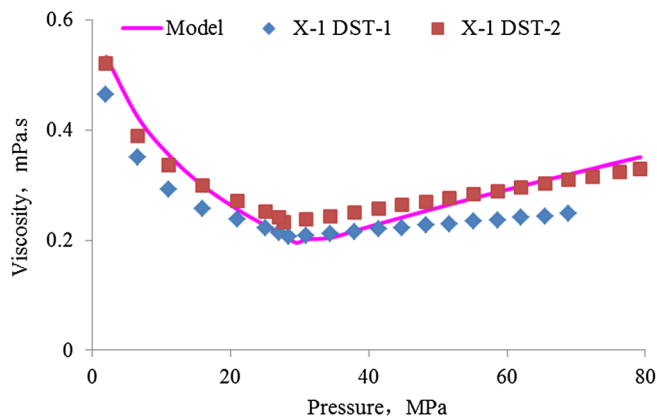
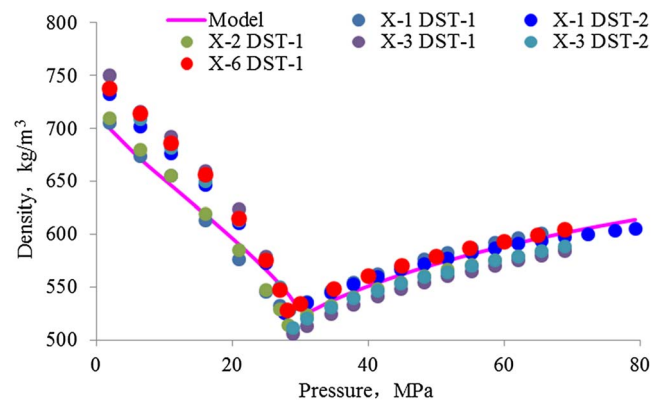
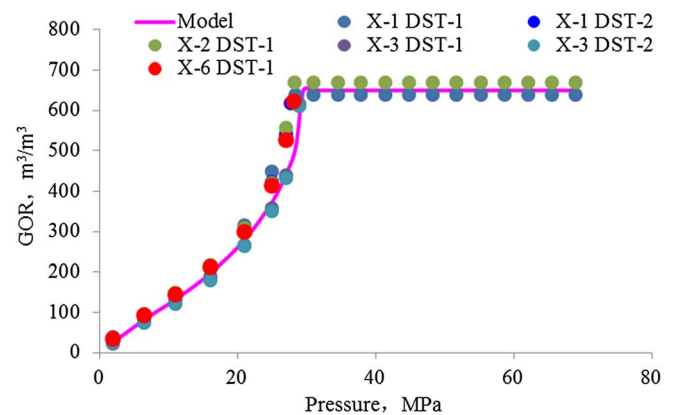
A detailed description of sample oils was obtained from experimental analysis. The oil was split into 14 components including 5 pseudocomponents for the heavy fraction. The Peng-Robinson Equation of State (EoS) was selected to predict thermodynamic properties. These component properties (critical pressure P_c , critical temperature T_c , and acentric factor ω) of heavy components were adjusted to match experimental data which include CCE and DL. The regression procedure of Agarwal *et al.* (1990) was used in the data matching. The oil viscosity, oil density and GOR calculated with 14 components are reported in Figures 2, 3 and 4 respectively showing good agreement with these experimental data. Figure 5 shows the discrepancies between post-match and pre-match of P – T phase diagrams. It is obvious that the P – T phase diagram after matching is enlarged and the saturation pressure at the reservoir temperature of 98 °C shows excellent agreement. A 14-component data set of thermodynamic properties was generated (Tab. 2). This is very useful in evaluating mechanisms of miscibility development of the acid gas injection.

3 Evaluation on mechanisms of vaporizing and condensing gas drive

Gas injection into a petroleum reservoir can be simulated using a cell-to-cell calculation presented by Metcalfe *et al.* (1973) and Pederson *et al.* (1986). This method simulates a number of cells of equal volumes in a series as shown in Figure 6. The temperature and the pressure are the same in each cell, and the volume is kept constant. Initially all

Table 1. Composition of oil and two types of injection gas.

Component	Crude oil	Produced gas	Deprived C ₃ ⁺
H ₂ S	0.151	0.15905	0.168
CO ₂	0.0413	0.05463	0.058
N ₂	0.00835	0.01164	0.013
C ₁	0.4703	0.63579	0.669
C ₂	0.073	0.08538	0.092
C ₃	0.0415	0.03426	0
C ₄	0.03052	0.01386	0
C ₅	0.02061	0.00386	0
C ₆	0.0165	0.00105	0
C ₇ -C ₉	0.0538	0.00048	0
C ₁₀ -C ₁₅	0.05532	0	0
C ₁₆ -C ₂₁	0.02081	0	0
C ₂₂ -C ₂₇	0.00882	0	0
C ₂₈ ⁺	0.00817	0	0

**Fig. 1.** Surface oil and gas separation process.**Fig. 2.** Oil viscosity curves and their fitting.**Fig. 3.** Oil density curves and their fitting.**Fig. 4.** GOR curves and their fitting.

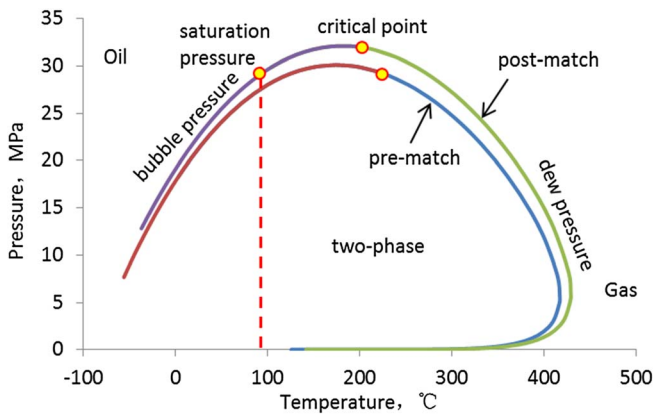
the cells contain the same fluid compositions. A specified amount of gas is added to cell 1. A flash calculation is performed in each cell when mixing takes place and thermodynamic equilibrium is attained. After mixing of the injected gas and the cell fluid, the excess volume from cell 1 is transferred to cell 2. The excess volume from cell 2 is transferred to cell 3, etc.

Pseudoternary diagrams are commonly used to decide whether or not miscibility has been achieved. Based on 14 pseudocomponents of the petroleum mixture, the composition of this mixture is represented using three groups of components, C₁+N₂, C₂-C₅+CO₂+H₂S and C₆⁺. In order to use a pseudoternary diagram in connection with a cell-to-cell method, the following steps are used to calculate the MMPs and generate pseudoternary diagrams for MCM processes at a given temperature:

1. Choose a range of pressures.
2. Gas is added to oil at specified gas to oil molar ratio increments and flash calculations are performed until two-phase region is detected.
3. Using the first point in the two-phase region detected in step 2, the flashed liquid is mixed with the original gas at the specified gas to liquid ratio and the flash

Table 2. Thermodynamic properties of the pseudocomponents.

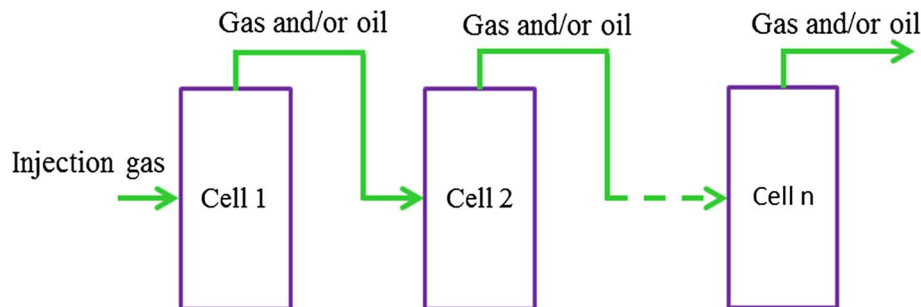
Component	M_w (kg/mol)	T_c (K)	P_c (atm)	V_c (m ³ /kg · mole)	Z_c	Boil (°C)	ω	Parachor
H ₂ S	34.1	373.2	88.20	0.099	0.284	-60.4	0.100	80.1
CO ₂	44.0	304.2	72.80	0.094	0.274	-78.5	0.225	78.0
N ₂	28.0	126.2	33.50	0.090	0.290	-195.8	0.040	41.0
C ₁	16.0	190.6	45.40	0.099	0.287	-161.5	0.008	77.0
C ₂	30.1	305.4	48.20	0.148	0.285	-88.7	0.098	108.0
C ₃	44.1	369.8	41.90	0.203	0.280	-42.1	0.152	150.3
C ₄	58.1	419.8	37.02	0.257	0.277	-4.1	0.188	187.3
C ₅	72.2	464.8	33.35	0.305	0.267	31.8	0.239	228.2
C ₆	86.0	507.5	32.46	0.344	0.268	63.9	0.275	250.1
C ₇ -C ₉	106.5	568.2	29.21	0.418	0.262	116.0	0.346	307.3
C ₁₀ -C ₁₅	161.7	664.1	21.82	0.622	0.249	210.5	0.523	452.2
C ₁₆ -C ₂₁	250.8	761.0	15.63	0.932	0.233	314.1	0.758	659.2
C ₂₂ -C ₂₇	325.9	824.4	12.29	1.183	0.215	388.0	0.942	806.6
C ₂₈ ⁺	476.1	924.0	8.76	1.616	0.187	505.6	1.180	1006.9

**Fig. 5.** P - T phase diagrams.

calculation is performed. This process simulates a condensing gas drive process, and generates the portion of the phase envelope.

4. The procedure is repeated until the liquid composition is the same as the vapor composition and MMP is the pressure at which this occurs.
5. If it is not true, then the pressure is increased to a new value and the steps 2-4 are repeated.
6. The procedure is the same for a vaporizing drive process except the third step, where the flashed vapor is mixed with the original oil at the specified gas-oil mixing ratio and then flash calculation is performed.

In our work, the gases that have been hypothesized to be injected into the reservoir are gases which are originated from the separator gas produced from this reservoir itself, as it is available from surface facilities. To further study the effect of gas compositions, removing all C₃⁺ fraction of separator gas has been considered as a possible candidate. At the same time, to gain an understanding of the mechanisms of vaporizing and condensing gas drive, mixtures of CO₂ and H₂S of varying composition with CH₄ injection gas are evaluated through simulation.

**Fig. 6.** Schematic diagram of cell-to-cell simulation.

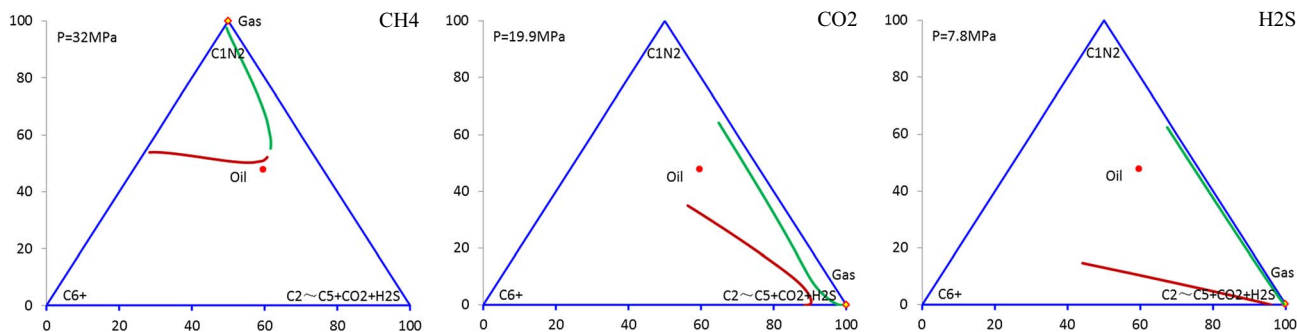


Fig. 7. Calculated pseudoternary diagrams with pure CH₄, CO₂ and H₂S injection respectively.

3.1 CH₄/CO₂/H₂S solvent

3.1.1 Pure CH₄/CO₂/H₂S

The pseudoternary diagrams for pure CH₄, CO₂ and H₂S injection were calculated using the cell-to-cell approach. These phase envelopes are quite different when MCM was achieved. A bell-shaped phase envelope was formed for pure CH₄, a distorted hourglass shape for CO₂ and a triangle shape for H₂S shown in Figure 7. MCM of pure CO₂ injection (19.9 MPa) is lower than that of pure CH₄ injection (32 MPa), and higher than that of pure H₂S gas (7.8 MPa). The simulation results demonstrated that the sour gas containing CO₂ and H₂S achieves miscibility easier than CH₄ by the vaporization of light ended hydrocarbons. The pressure-temperature phase diagrams for these three gases were presented in Figure 8. Of course, pure H₂S injection in real oilfields is impractical because of its hyper-toxicity. Simulation calculations of pure H₂S injection are only for purpose of comparison and evaluation of miscible mechanisms.

3.1.2 Comparison of CH₄/CO₂ and CH₄/H₂S solvent

From Figure 9, the saturation pressures of CH₄/CO₂ solvent initially increase then decrease, while the saturation pressure curve of pure CO₂ injection keeps decreasing and the curve of pure CH₄ gas increase rapidly. The maximum point of the curve is the FCM except CH₄. Calculated FCMs of CH₄/CO₂ solvents containing CH₄ being 0 mole, 0.25 mole, 0.5 mole and 0.75 mole were 29.5 MPa, 30.5 MPa, 41.2 MPa and 62.8 MPa, respectively. An increase in the amount of CO₂ in the injected gas would decrease the FCM pressures as expected. However, with CH₄ concentrations higher than a threshold value of 0.5 mole, incremental FCM pressure value would rise noticeably. These pressure-composition diagrams indicate a vaporizing process for CH₄/CO₂ solvents containing CH₄ being 0.25 mole, 0.5 mole, 0.75 mole and pure CH₄, while condensing process for pure CO₂.

Multiple contact calculations were then performed with 14 components for CH₄/CO₂ solvents (CO₂ equals 0.75 mole, 0.5 mole and 0.25 mole). The corresponding pseudoternary diagrams are shown in Figure 10. MCM pressures of three mixtures gases are very close. But phase envelopes of pseudoternary diagrams between CO₂ 0.5 mole

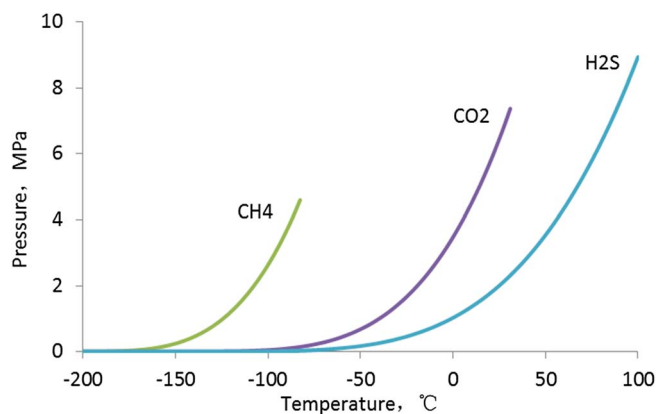


Fig. 8. P - T phase diagrams with pure CH₄, CO₂ and H₂S gases.

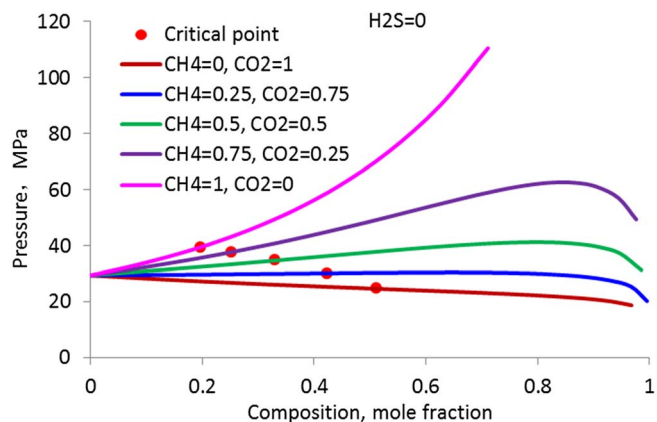


Fig. 9. Pressure-composition diagrams for CH₄/CO₂ solvent.

and 0.25 mole are opposite directions. As CO₂ concentrations increase, MCM pressures would decrease slowly. By comparison, the FCM for all injected gas compositions was achieved at higher pressures and it appears that the variation of the injected gas composition had clear effects on FCM pressures.

The trend is very similar for pressure-composition diagrams of CH₄/H₂S solvent plotted in Figure 11. Calculated FCMs of CH₄/H₂S solvents consisting of various

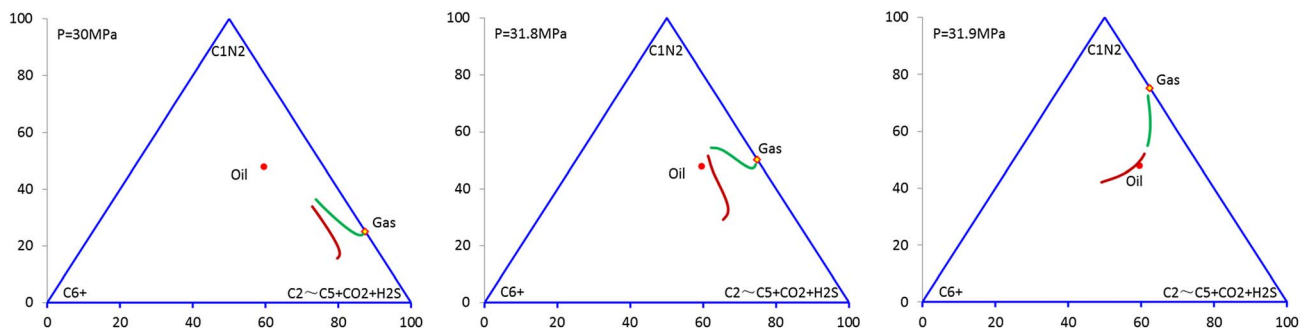


Fig. 10. Calculated pseudoternary diagrams with CH₄/CO₂ solvent (CO₂ = 0.75, 0.5, 0.25 mole).

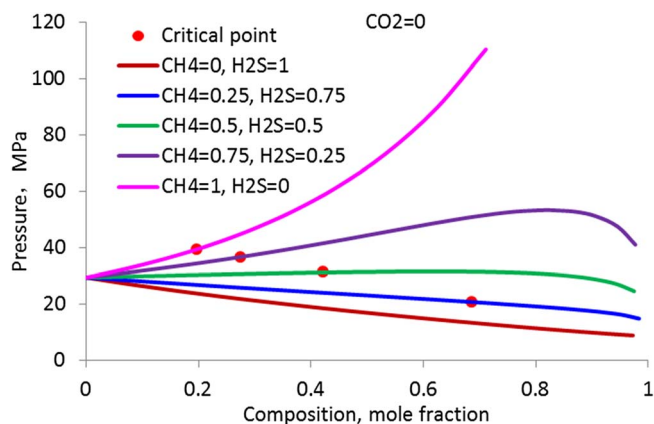


Fig. 11. Pressure-composition diagrams for CH₄/H₂S solvent.

proportions of CH₄ being 0, 0.25, 0.5 and 0.75 mole were 29.5 MPa, 29.5 MPa, 31.8 MPa and 53.7 MPa respectively. The shape of phase envelopes of pseudoternary diagrams for CH₄/H₂S are different from CH₄/CO₂, especially the CH₄/H₂S (H₂S 0.75 mole) solvent appears triangle shape similar to pure H₂S (Fig. 12).

3.1.3 CH₄/CO₂/H₂S solvent

When the CH₄ concentration equals 0 mole, pressure-composition diagrams for different mole fractions of CO₂ and H₂S have a decreasing trend showed in Figure 13.

As the amount of CO₂/H₂S solvent injected increases, the saturation pressure is reducing. The increase of H₂S concentrations in the injected gas decreases the MCM pressures for the reservoir oil by 0.1205 MPa/mol% (Fig. 14). FCM pressures of all mixtures are 29.5 MPa. When the CH₄ mole fraction raised to 0.25 mole, pressure-composition diagrams for different mole fractions of CO₂ and H₂S change from CO₂ 0.75 mole to 0 mole plotted in Figure 15. As CO₂ concentration increases, the decreasing amplitude becomes flattened then decreases rapidly. An increase in the amount of H₂S in the injected gas would decrease MCM pressures as expected. FCM pressures would level off and attain a constant value of 29.5 MPa when H₂S concentration is higher than a threshold value of 0.15 mole (Fig. 16). When the CH₄ concentration equals 0.5 mole, pressure-composition diagrams for different mole fractions of CO₂ and H₂S vary noticeably. These shapes of pressure curves are typically increasing then decreasing and the maximum point appears (Fig. 17). Simulation results demonstrated that MCM pressures decrease relatively small, while FCM pressures decrease with H₂S increase (Fig. 18). The trend for 0.5 mole of CH₄ is very similar to 0.75 mole of CH₄. But the maximum points become larger (Fig. 19). MCM pressures of all mixtures equal 31.9 MPa and FCM pressures decrease with H₂S increase (Fig. 20).

3.2 Comparison of produced gas and deprived of its C₃⁺

The main difference between produced gas and deprived of its C₃⁺ is the light component content, which the

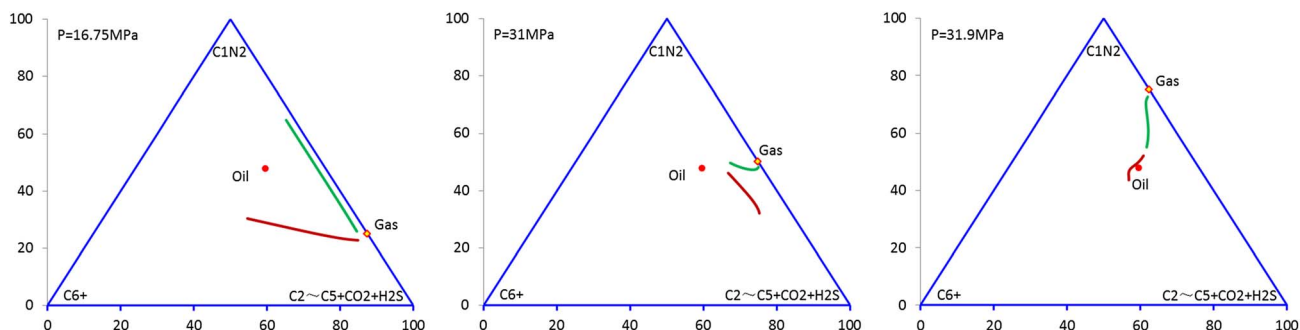


Fig. 12. Calculated pseudoternary diagrams with CH₄/H₂S solvent (H₂S = 0.75, 0.5, 0.25 mole).

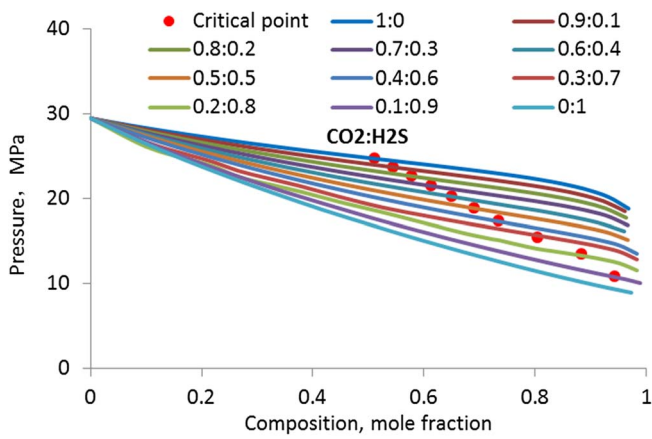


Fig. 13. Pressure-composition diagrams for different mole fractions of CO₂ and H₂S with CH₄ = 0 mole.

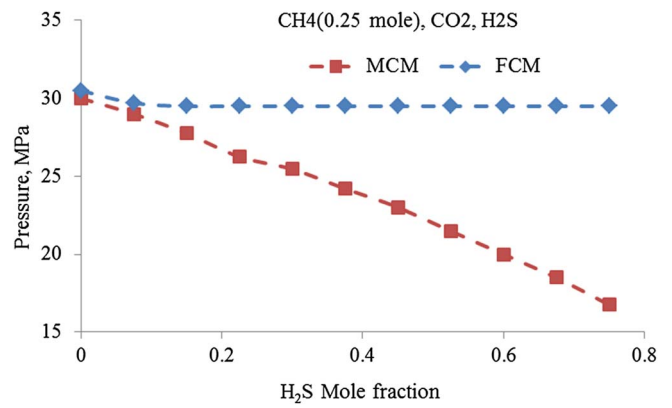


Fig. 16. MCM and FCM pressures for different mole fractions of CO₂ and H₂S with CH₄ = 0.25 mole.

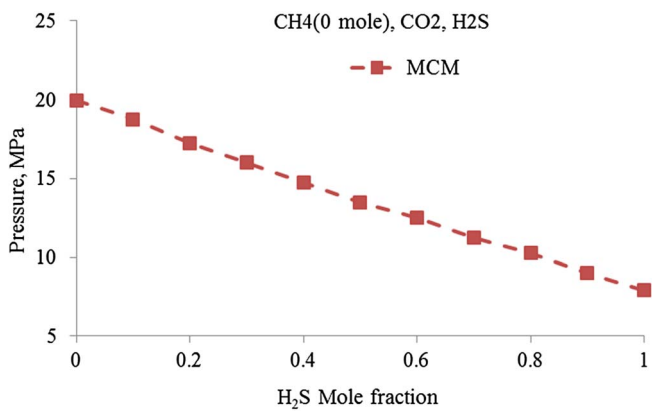


Fig. 14. MCM pressures for different mole fractions of CO₂ and H₂S with CH₄ = 0 mole.

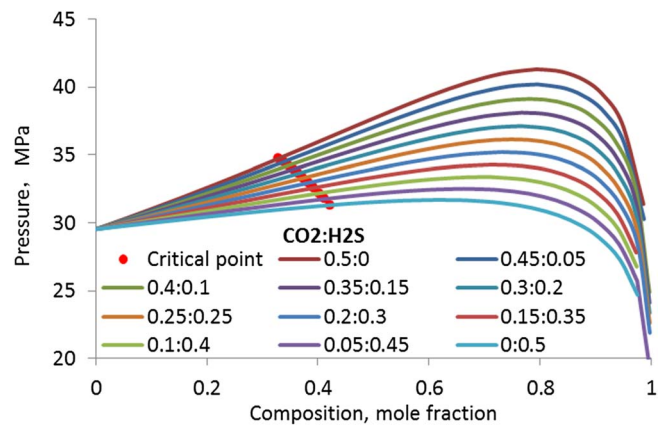


Fig. 17. Pressure-composition diagrams for different mole fractions of CO₂ and H₂S with CH₄ = 0.5 mole.

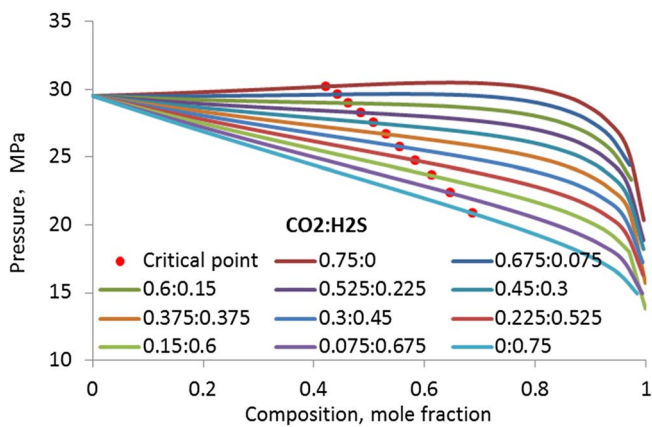


Fig. 15. Pressure-composition diagrams for different mole fractions of CO₂ and H₂S with CH₄ = 0.25 mole.

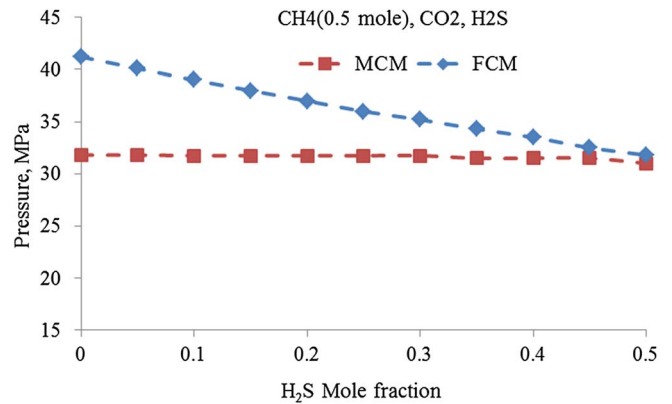


Fig. 18. MCM and FCM pressures for different mole fractions of CO₂ and H₂S with CH₄ = 0.5 mole.

concentrations of light components of the latter is higher than the former (Tab. 1). The pressure-composition diagram of a reservoir oil/injection gas system is a valuable

tool to help identify the process mechanisms. Simulation results of pressure-composition diagrams for two types of injection gas are plotted in Figure 21. Plots indicate a

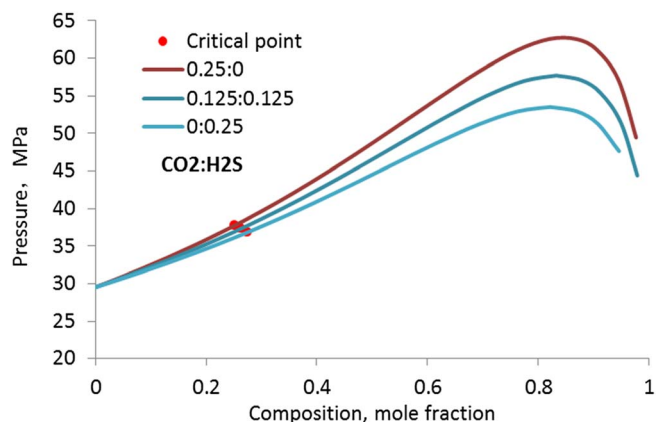


Fig. 19. Pressure-composition diagrams for different mole fractions of CO_2 and H_2S with $\text{CH}_4 = 0.75$ mole.

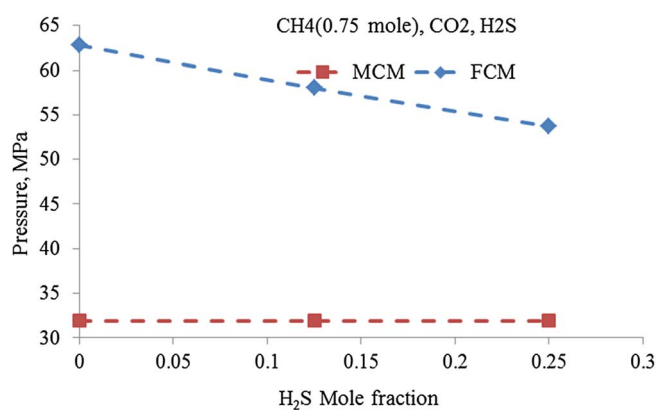


Fig. 20. MCM and FCM pressures for different mole fractions of CO_2 and H_2S with $\text{CH}_4 = 0.75$ mole.

vaporizing process rather than a condensing process since the critical point is to the left of the cricondenbar. The process is first contact miscible at 47 MPa and 52 MPa for

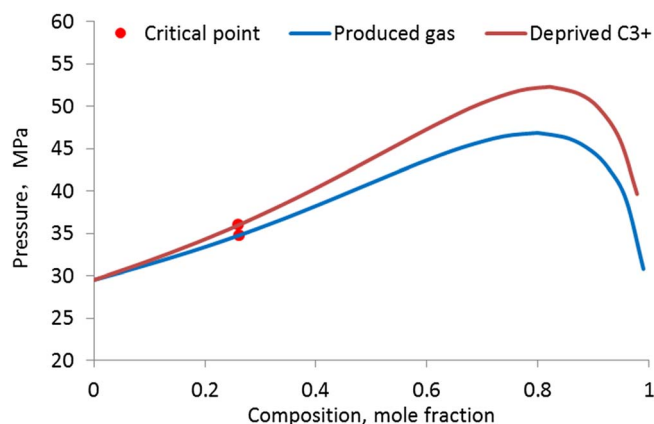


Fig. 21. Calculated pressure-composition diagrams for two types of injection gas.

produced gas and deprived C_3^+ gas respectively. It is also clear that the saturation pressure curve of the deprived C_3^+ gas is higher than produced gas. The multiple contact pseudoternary diagrams for these two types of injection gas/reservoir oil systems were calculated at several pressures (Figs. 22 and 24). The left figure in Figure 22 for produced gas/reservoir oil system indicates a vaporizing process at 30 MPa because the envelope for this process is not closed and forms an hourglass shape. Therefore miscibility was not achieved. As pressure is increased, the right figure in Figure 22 shows the diagram at 32 MPa. In this case, the phase envelope closes indicating a multiple contact miscible with the oil and the process becomes essentially a vaporizing process. Miscibility is generated by backward contacts of the equilibrium liquid phase with fresh gas (Fig. 23). So the MCM is 32 MPa.

However, from Figure 24, pseudoternary diagrams for reservoir oil/deprived C_3^+ gas system is obviously different from reservoir oil/produced gas system. The 20.25 MPa of MCM for deprived C_3^+ gas is lower than produced gas.

Due to the volatile nature of the sample oil, the full miscibility would achieve at the reservoir pressure of 77.7 MPa.

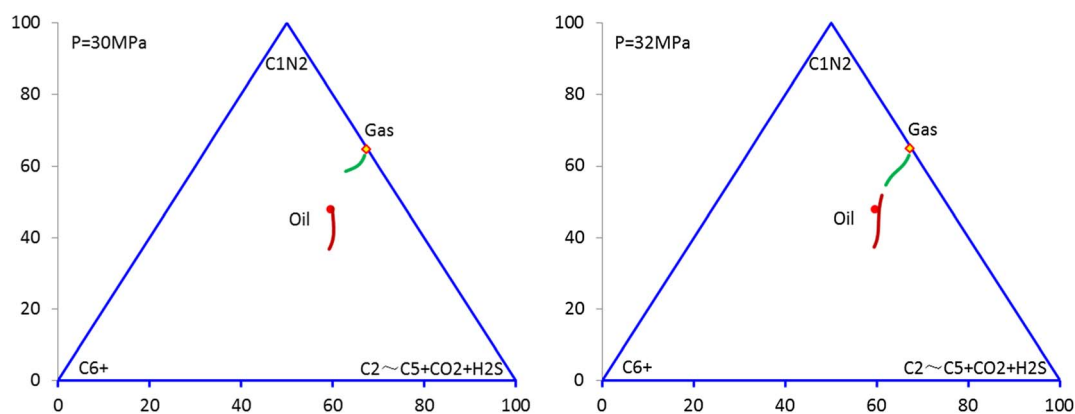


Fig. 22. Pseudoternary diagrams from multiple contact calculations for reservoir oil/produced gas system at 98°C .

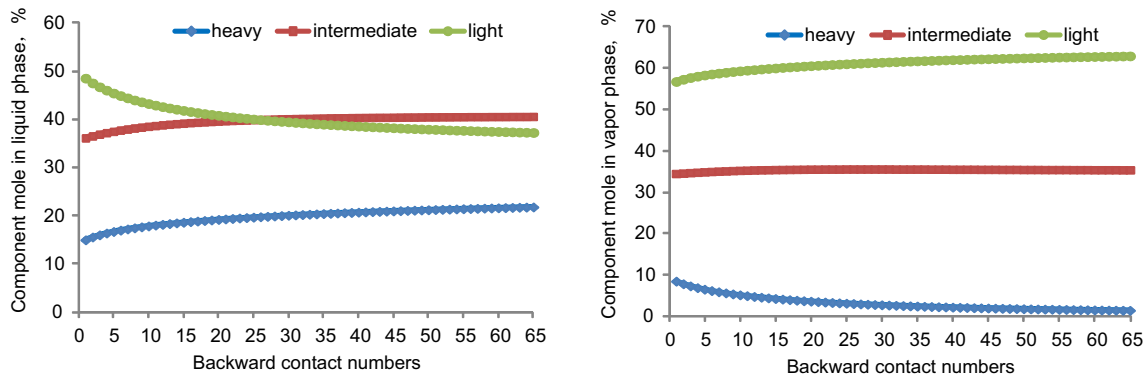


Fig. 23. Backward contact of produced gas.

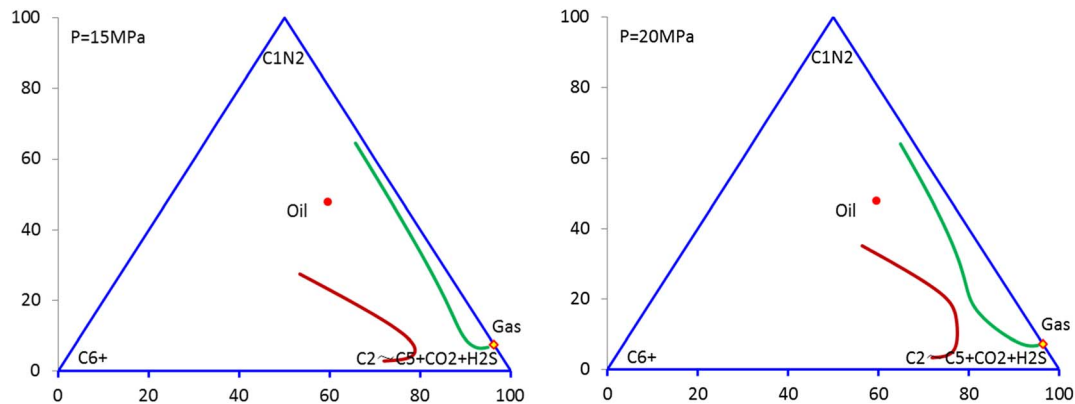


Fig. 24. Pseudoternary diagrams from multiple contact calculations for reservoir oil/deprived C_3^+ gas system at 98 °C.

4 Conclusion

A 14-component compositional simulation model was built after matching laboratory PVT data. The pressures of FCM and MCM could decrease favorably as the CO_2 and/or H_2S concentration increased in the injected stream. The envelope shape of pseudoternary diagrams relies on the composition of the injected gas. The following conclusions can be made from the previous results.

The mechanism of recovery can be identified using pressure-composition diagrams and pseudoternary diagrams generated with cubic EoS which have been tuned to match experimental data. Calculated pressures of FCM and MCM are feasible using the cell-to-cell method.

Different injection gases of $CH_4/CO_2/H_2S$ have characteristic shapes of the envelope of pseudoternary diagrams: bell shape, hourglass shape and triangle shape. This is very useful in identifying miscible mechanisms.

The volatile oil showed a nearly linear MCM pressures with mole fraction for each gas component mixed with $CH_4/CO_2/H_2S$. CO_2 and H_2S can reduce the pressure of FCM and MCM. As the CH_4 mole fraction increases, MCM pressures of mixtures would increase. FCM pressures are higher than MCM pressures. Moreover, as the CH_4 concentrations increase, the incremental FCM pressures are bigger.

Acknowledgments. The authors greatly acknowledge the financial support from the Important National Science and Technology Specific Projects of China (Grant No. 2017ZX05030-002).

References

- Abrishami Y., Hatamian H. (1996) *Phase behaviour of fluids in multiple contact processes with CO_2 , N_2 and their mixture*. SPE-36295.
- Agarwal R.K., Li Y.K., Nghlem L. (1990) A regression technique with dynamic parameter selection for phase-behavior matching, *SPE Reserv. Eng.* **5**, 01, 115–120.
- Al-Hadhrami A.K., Davis D.W., Deinum G., Soek H. (December 2007) The design of the first miscible sour gasflood project in Oman, *International Petroleum Technology Conference*, Dubai, U. A. E., 4–6 December 2007. Document ID: IPTC-11396.
- Belhaj H., Abukhalifeh H., Javid K. (2013) Miscible oil recovery utilizing N_2 and/or HC gases in CO_2 injection, *J. Pet. Sci. Eng.* **111**, 144–152.
- Gardner J.W., Orr F.M., Patel P.D. (1981) The effect of phase behavior on CO_2 -flood displacement efficiency, *J. Pet. Technol.* 2067–2081.
- Johns R.T., Ahmadi K., Zhou D., Yan M. (2010) A practical method for minimum miscibility pressure estimation of contaminated CO_2 mixtures, *SPE Reserv. Eval. Eng.* **13**, 764–772.

- Johns R.T., Yuan H., Dindoruk B. (2002) *Quantification of displacement mechanisms in multicomponent gasfloods*. SPE-77696.
- Luo E.H., Hu Y.L., Li B.Z., Zhu W.P. (2013a) Practices of CO₂ EOR in China, *Special Oil Gas Reserv.* **20**, 2, 1–7. (in Chinese).
- Luo E.H., Hu Y.L., Li B.Z., Wang J.L., Wang Z.B. (2013b) Methods of improving sweep volume by mobility control of CO₂ flood in foreign countries, *Oilfield Chem.* **30**, 4, 613–619. (in Chinese).
- Luo E.H., Zhao L., Fan Z.F., Wang J.J. (2018) *A study of PVT physical properties characteristic and compositional numerical simulation for sour gas injection*. In review.
- Metcalfe R.S., Fussell D.D., Shelton J.L. (1973) A multicell equilibrium separation model for the study of multiple contact miscibility in rich-gas drives, *SPE J.* **13**, 03, 147–155.
- Nutakki R., Hamoodi A.N., Li Y.-K., Nghiem L.X. (1991) *Experimental analysis, modelling, and interpretation of recovery mechanisms in enriched-gas processes*. SPE-22634.
- Pederson K.S., Fjellerup J., Thomassen P., Fredenslund A. (1986) *Studies of gas injection into oil reservoirs by a cell-to-cell simulation model*. SPE-15599.
- Stalkup F.I. (1987) *Displacement behavior of the condensing/vaporizing gas drive process*. SPE-16715.
- Tang Y., Sun L., Zhou Y.Y., Li S.L., Sun L.T., Du Z.M. (2005) Mechanism evaluation of condensing/vaporizing miscible flooding with hydrocarbon-rich gas injection, *Pet. Explor. Dev.* **32**, 2, 133–136.
- Urazgaliyeva G., King G.R., Darmentaev S., Tursinbayeva D., Dunger D., Howery R., Zalan T., Lindsell K., Iskakov E., Turymova A., Jenkins S., Walker C., Bateman P., Aitzhanov A. (2014) Tengiz sour gas injection project: An update, *SPE Annual Caspian Technical and Exhibition*, Astana, Kazakhstan, 12–14 Bivermber 2014. Document ID: SPE-172284.
- Wang S., Yeskaiyr B., Walker C. (October 2014) A sector model for IOR/EOR process evaluation, *SPE Annual Technical Conference and Exhibition*, Amsterdam, The Netherlands, 27–29 October 2014. Document ID: SPE-170605.
- Zhang C.S., Fan Z.F., Xu A.Z., Zhao L., Zhao L.D., Luo E.H. (2017) Study on miscible mechanism of recycle dissolved gas in volatile oil reservoir with acid gas, *Reserv. Eval. Dev.* **7**, 2, 41–46.
- Zick A.A. (1986) *A combined condensing/vaporizing mechanism in the displacement of oil by enriched gases*. SPE-15493.